Heliyon 9 (2023) e20054

Contents lists available at ScienceDirect

Heliyon

journal homepage: www.cell.com/heliyon

Holographic photopolymerization combined to microfluidics for the fabrication of lab-in-lab microdevices and complex 3D micro-objects

Abhijeet Lale [a], Colman Buckley [b], Vincent Kermène [b,**], Agnès Desfarges-Berthelemot [b], Frédéric Dumas-Bouchiat [d], Emmanuel Mignard [c], Fabrice Rossignol [d,*]

[a] Lithoz GmbH, Mollardgasse 85a/2/64-69, 1060, Wien, Austria
[b] XLIM, CNRS UMR 7252, University of Limoges, 123 Av. Albert Thomas, 87000, Limoges, France
[c] ISM, CNRS UMR 5255, University of Bordeaux, 351 Cr de la Libération, 33405, Talence, France
[d] IRCER, CNRS UMR 7315, University of Limoges, 12 rue Atlantis, 87068, Limoges, France

ARTICLE INFO

Keywords:
Holographic photopolymerization
Microfluidic devices
3D-fabrication
Acrylate
Resins
Hydrogels

ABSTRACT

We show here brand-new possibilities of lab-in-lab fabrication while combining holographic photopolymerization and microfluidics. One shot real-time 3D-printing can produce 3D architectured microchannels, or free-standing complex micro-objects eventually in flow. The methodology is very versatile and can be applied to *e.g.*, acrylate resins or hydrogels.

1. Introduction

A lack of easy scalable manufacturing techniques has been a roadblock in uptake of microfluidic technologies from academic research to commercially viable products. The capabilities of existing methods for fabricating devices, such as etching (for glass and silicon), embossing, and injection molding (for thermoplastics), are constrained by the diversity of features they can produce. ([1–3]). The paradigm of bottom-up building, also known as additive manufacturing (AM), is revolutionizing three-dimensional (3D) fabrication ([4,5]). Most commonly used AM techniques are either based on point-by-point or layer-by-layer deposition which allows broad geometric versatility. This offers an ability to produce complex structures that are not possible to manufacture using subtractive methods ([6–8]).

Current AM processes create 3D geometries by way of iterative 1D or 2D unit operations ([9,10]). Transitioning from 2.5D structures (which have differing widths but identical depth) to 3D structures results in extended processing durations and a decrease in achievement rates. Other earlier techniques like soft lithography, although today well developed, require dust-free environment. Hence, they have a high cost and are time-consuming. Other manufacturing techniques like molding, fused filament fabrication (FFF), multijet modelling (MJM) and conventional laser stereolithography have a resolution starting typically from 20 μm (there are however

* Corresponding author.
** Corresponding author.
E-mail addresses: vincent.kermene@xlim.fr (V. Kermène), fabrice.rossignol@unilim.fr (F. Rossignol).

https://doi.org/10.1016/j.heliyon.2023.e20054
Received 13 April 2023; Received in revised form 20 August 2023; Accepted 9 September 2023
Available online 11 September 2023
2405-8440/© 2023 The Authors. Published by Elsevier Ltd. This is an open access article under the CC BY-NC-ND license (http://creativecommons.org/licenses/by-nc-nd/4.0/).

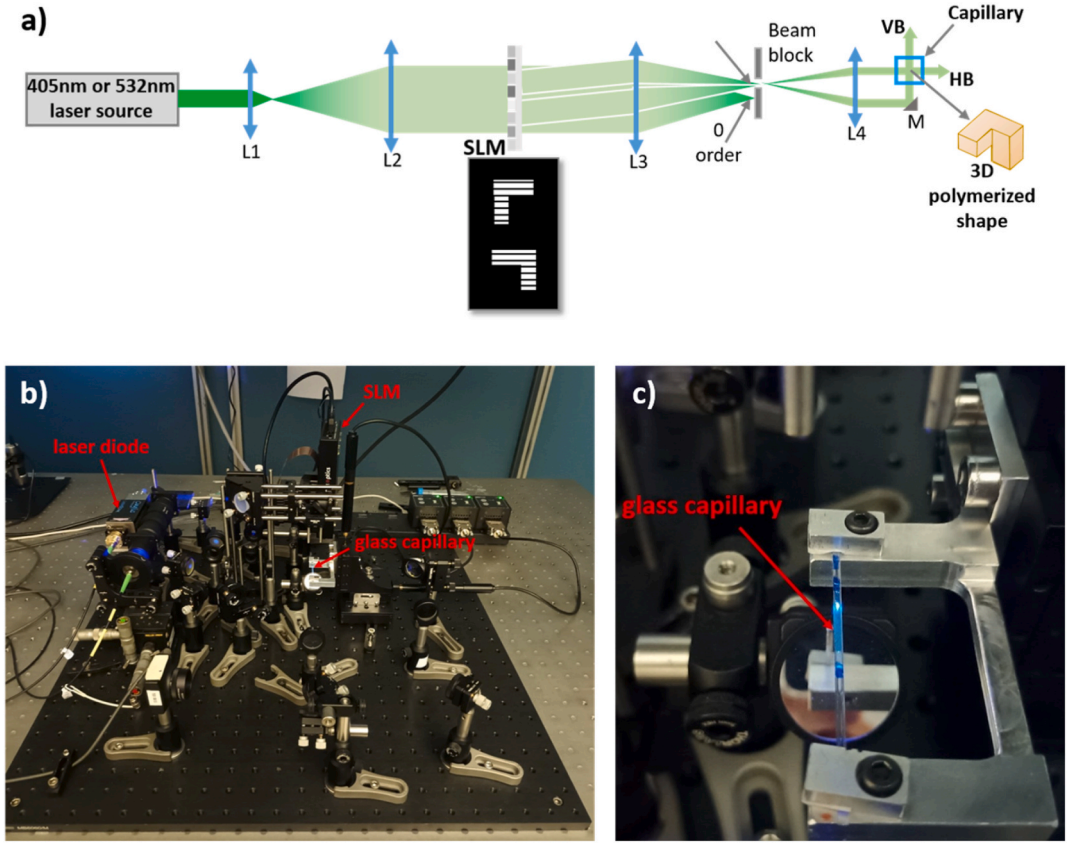

Fig. 1. a) Diagram of the experimental setup. The afocal system (L1, L2) expands the beam of the laser diode. The hologram displayed on the SLM (spatial light modulator) splits the large laser beam in two shaped beams. A beam block in the SLM Fourier plane selects only the first order of both diffracted beams. The second afocal system (L3, L4) images the SLM into the capillary. VB, vertical shaped beam. HB, horizontal shaped beam. M, mirror. b) Photography of the experimental setup equipped here with the blue laser (405 nm). c) Zoom on the glass capillary under laser beam illumination.

micro-stereolithographic systems with better resolutions [11]). Other techniques like nanoimprint lithography, E-beam lithography have resolutions typically from 5 nm to 600 nm. In addition, in the case of stereolithography and FDM, the process is quite slow since it follows a layer-by-layer approach and a pixel-by-pixel approach, respectively.

These methods restrict output, deteriorate surface smoothness, limit geometric potential, amplify demands for subsequent processing, which in turn escalates expenses and time commitments. Furthermore, they might induce variations in properties such as mechanical strength. Introducing a manufacturing method that can create all points within any given 3D shape concurrently would present an alternative approach to tackle these challenges and supplement established AM techniques. Several new studies based on Computed Axial Lithography (CAL) and Xolography ([12–15]) offer ways to avoid problems created by traditional layer-by-layer approach by providing a volumetric printing solution. A 3D object is fabricated by irradiating a liquid photopolymer volume from the side with computed light patterns representing projections of the object to fabricate. However, none of these methods provide possibility of volumetric printing inside a microfluidic channel with a micron size resolution.

2. Materials and methods

Here we describe the use of a new photopolymer based additive manufacturing technique that allows formation of 3D volumetric structures as single units, *i.e.*, a single exposure polymerization leading to complete build-up of 3D structures in one shot to develop microfluidic devices inside square capillaries with micron size resolutions. The method can also be adapted as a continuous printing process for micro-parts manufacturing. The printing or manufacturing process is executed by overlaying patterned optical fields generated from multiple light beams projected into a photosensitive resin. Alternatively, a single patterned optical beam can be utilized, as explained in the work by Kelly et al. [16].

2.1. Holographic printing set-up

The structuration of the light beams is performed by a holographic projection system [8] schematically detailed in Fig. 1, using a

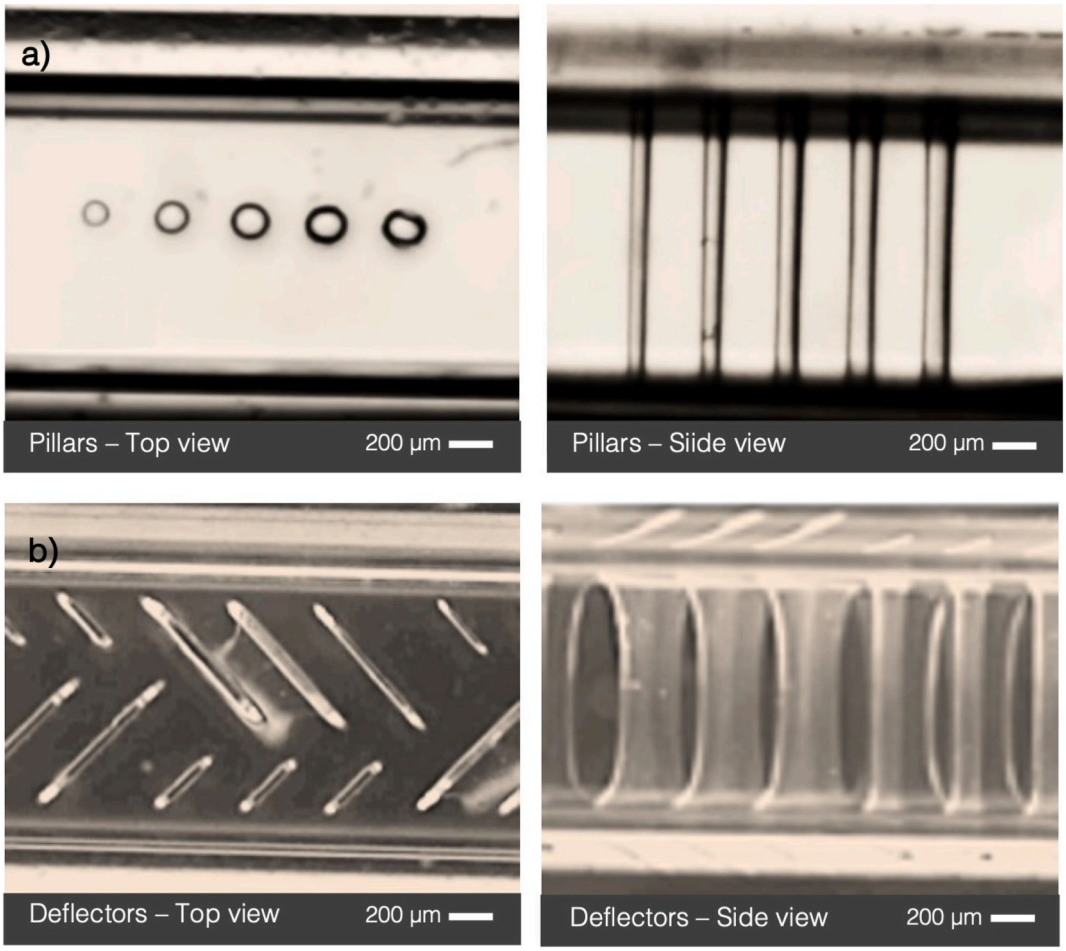

Fig. 2. a) pillars of varying diameters and b) deflectors to be used as fluid mixers, both anchored inside a microfluidic channel of a 1 mm × 1 mm cross section (irradiation: green laser power of 1 W and exposure time of 0.4 s).

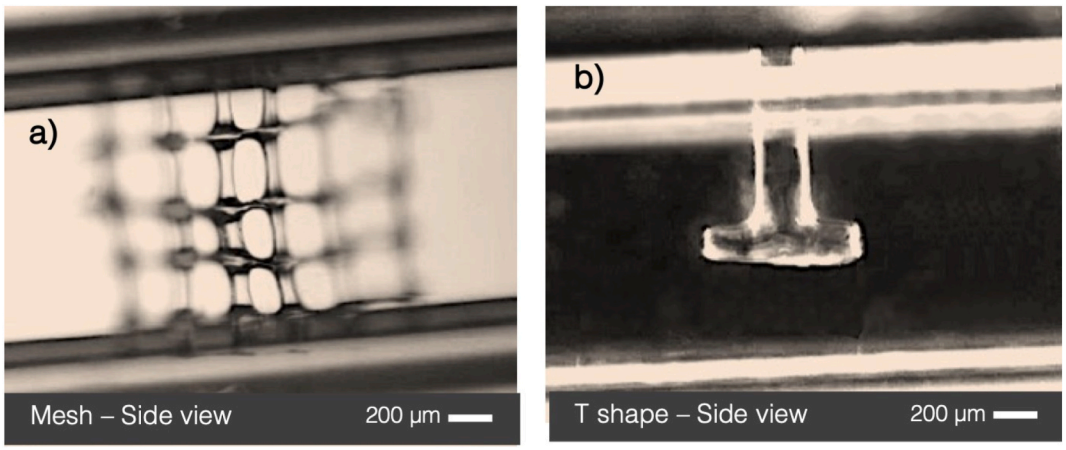

Fig. 3. Supported true single shot 3D shapes: a) mesh inclined at 45° to the channel axis and b) T shape, both anchored inside a microfluidic channel of a 1 mm × 1 mm cross section (irradiation: green laser power of 1 W and exposure time of 0.4 s).

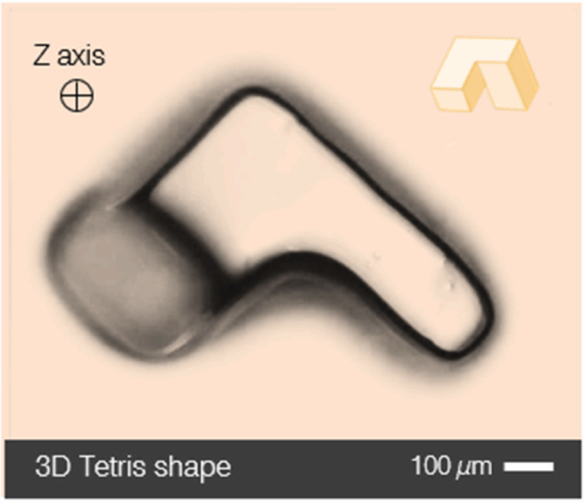

Fig. 4. Example of an unsupported true 3D Tetris shape fabricated using a sequentially interrupted flow (irradiation: green laser power of 1 W and exposure time of 0.4 s).

phase only Spatial Light Modulator (SLM, Meadowlark P1920-0532-HDMI), seeded by a continuous wave green laser (532 nm) or blue laser diode (405 nm) depending on the photoinitiator. This optical system generates two shaped beams overlapping inside the square section capillary from orthogonal direction, to polymerize a 3D form. The SLM displays a computed hologram, two patterns related to the shaped beams, modulated by a phase grating (grating period 10 pixels of 9.2 μm size). In the Fourier plane of the SLM, a filter blocks the unwanted diffraction orders. An afocal system images through this filter the two diffracted beams into the capillary. Both beams overlap in a 1 mm^3 volume, matching the inner part of the square capillary of 1 mm^2 cross section (10 cm long). The 2 mm diameter of the beam block pinhole limits the resolution of the shaped beam in the capillary to 30 μm (Rayleigh criterion). Therefore, the shape and size of the beams of plane wavefront do not change along the capillary cross section. However, the resolution of the 3D polymerized shape can be smaller depending on the characteristics of the photopolymer and light exposure.

This optical system can be used with a single beam to polymerize a 2.5D structure all along the cross section of the capillary, either in the horizontal or the vertical axis. Then, the structure is anchored to the opposite walls of the capillary. Involving both shaped beams, the holographic projection system is able to generate true 3D form, anchored or not to the capillary walls, where the beams overlap.

2.2. Materials

The 3D printing system was experimented with different crosslinkable materials such as hydrogels, Polymer Derived Ceramics (not reported here) and acrylate resins. This is with these latter resins that the polymerized shapes shown in Figs. 2–4 were obtained. Exposures in this system were carried out in a resin volume of 0.1 ml contained in a 10 cm long silica glass square capillary with a 1 mm × 1 mm inner cross-section and 0.2 mm wall thickness bought from CM scientific, UK (VitroCom's Vitrotubes). The resin consisted of low molecular weight poly(ethylene glycol) diacrylate (PEGDA; Mn = 250 g/mol, Sigma-Aldrich, Germany), with 0.05–0.2% (w/w) of Bis(2,6-difluoro-3-(1-hydropyrrol-1-YL)phenyl) titanocene (Apollo Scientific, UK) as photoinitiator sensitive at the 532 nm wavelength of the laser source and 10–15% (w/w) of hydroquinone (Sigma Aldrich, Germany) as radical inhibitor. The process involved the manipulation of the laser power at the source and the exposure time. The two parameters are bundled into a single variable, the power-time product for the sake of simplicity. The process involves three key elements. First, structuration of the laser light beams such that all required locations in the resin, as per the shape, receive adequate power dose needed to stimulate simultaneously the polymerization throughout the all volume. Second, limitations on the axial resolution of the beams must be compensated by optimizing the lateral intensity profile of each beam. This optimization is also beneficial for depth-dependence of energy absorption in the resin. Lastly, we use polymerization inhibiting species to allow for the non-linearity necessary for "threshold" behavior in the polymerization process. Indeed, the role of molecular oxygen (O_2) dissolved in the resin is known to influence the polymerization inhibiting behavior. The successful feedstock formulations presented in this paper are the result of upstream optimizations which are themselves not reported. The criteria defining a good quality feedstock were the possibility to get polymerized features approaching 10 μm in size and, at the same time, able to sustain the post-process of washing without any failure when attached to the wall of the microfluidic channel.

2.3. Follow-up of the photopolymerization of acrylates by Raman

Raman spectroscopy was carried out using a 532 nm laser wavelength. A drop of feedstock material was placed on a microscope glass slide and the glass slide itself was placed in the holder position of an InVia Reflex spectrometer (Renishaw, UK). The laser in the Raman spectroscopy machine was used for dual purpose: *(i)* activating polymerization and *(ii)* measuring the changes in peak

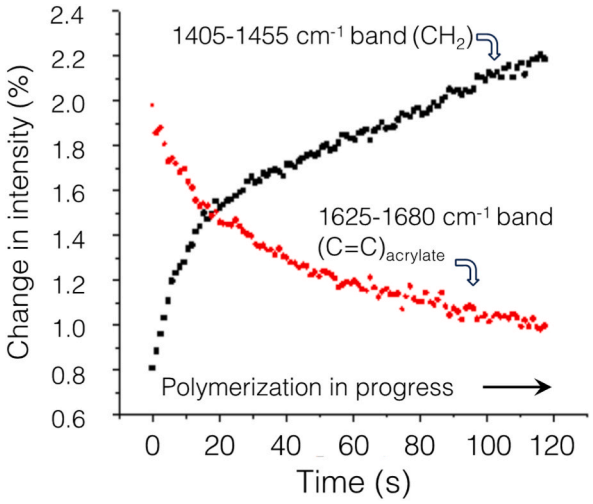

Fig. 5. Change in % of intensity of bands at 1625-1680 cm^{-1} and 1405-1455 cm^{-1} corresponding to (C═C) $_{acrylate}$ and CH_2 bonds, respectively, in PEG-DA subjected to photo-polymerization, as measured using Raman spectroscopy at 532 nm (100 mW laser, PEG-DA with 0.2% photo-initiator and 10% inhibitor). The exact conversion rate was not estimated.

intensities during the measurement.

The band at about 1625–1680 cm^{-1} corresponded to the strong signal of the carbon-carbon double bond of acrylates, while the one, weaker, characteristic of the CH_2 group was at about 1405–1455 cm^{-1}. The decreasing signal of the C═C is commonly used to monitor radical polymerizations, and we already did it with success as shown in one of our previous papers [17]. Here the exact conversion rate was not measured. The change in the CH_2 signal intensity relies to the fact that what changes with polymerization is that in the CH_2 vicinity there is an alkane bond and not an alkene anymore.

3. Demonstration of feasibility

3.1. Shaping ability

While combining a high-resolution flow control system (*e.g.*, Elveflow®, Elvesys, France) which is not shown in Fig. 1, the structures can be realized in a continuous or sequentially interrupted flow to allow for synchronization with external stimuli (*e.g.*, laser illumination or other processing steps). Beyond the synthesis of 3D objects in the static mode, the dynamic mode configuration (continuous flow + spatial modification of the polymerizable zone) makes it possible to consider the development of complex curved objects. Fig. 2a to b, Fig. 3a to b and Fig. 4 show various 2.5D, true 3D and a standalone 3D complex shape, respectively, that were prepared using this technique inside a 1 mm × 1 mm square silica capillary. In the specific case of 3D structures, the beam was split in two perpendicular beams. Importantly, there are no limitations on the dimensions of span, bridge, and cantilever components, and curves can be generated without encountering layering imperfections. These are notable hurdles in conventional additive manufacturing methods that build layer by layer. Additionally, there is no need for a supporting substrate during the construction process, although one can be employed if preferred. Most structures generated using this route are robust and within tolerance limits but detailed mechanical study on the structures is out of the scope of this paper. A preliminary study on a use of the architectured microfluidic channel of Fig. 2b as robust mixers for fluids was done as a proof of concept (not reported here).

Our studies indicate that structures can be generated inside the capillaries using exposure times ranging from 0.3 to 10 s and total incident power ranging from 10 mW to 40 mW. The smallest feature generated using this process is a cylindrical pillar with a diameter close to 15 μm. The smallest possible feature achievable using this technique is limited by the diffraction limit of the optical system, which is 30 μm for the current system. Although, we state the smallest possible feature printable to be close to 15 μm, there is likely a possibility to print features even smaller than 15 μm. This is achievable as the exposure time for certain shapes is very short (<0.5s) and the polymerization response of the feedstock is quite fast. If a high dose of power is provided for a very short duration, *i.e.*, less than that required for complete polymerization, it results in formation of features which are smaller than the actual size of the projected hologram. This hack to print features which are smaller than the resolution limit of the process works only with symmetric simple shapes.

Fig. 5 shows a percentage change in intensity of $(C{=}C)_{acrylate}$ and CH_2 bonds in PEG-DA measured using Raman spectroscopy. As already said, the Raman laser at 532 nm was used both to cause photopolymerization and to collect the Raman data (100 mW). It is clear from this graph that polymerization stabilizes after some time and does not reach 100% conversion. It also shows that the photopolymerization is non-linear, due to oxygen inhibition both from dissolved oxygen and presence of hydroquinone. The 3D shapes made with the 2 illumination beams exploit the non-linearity of the process highlighted in Fig. 5 to reach the polymerization threshold only in the target volumes.

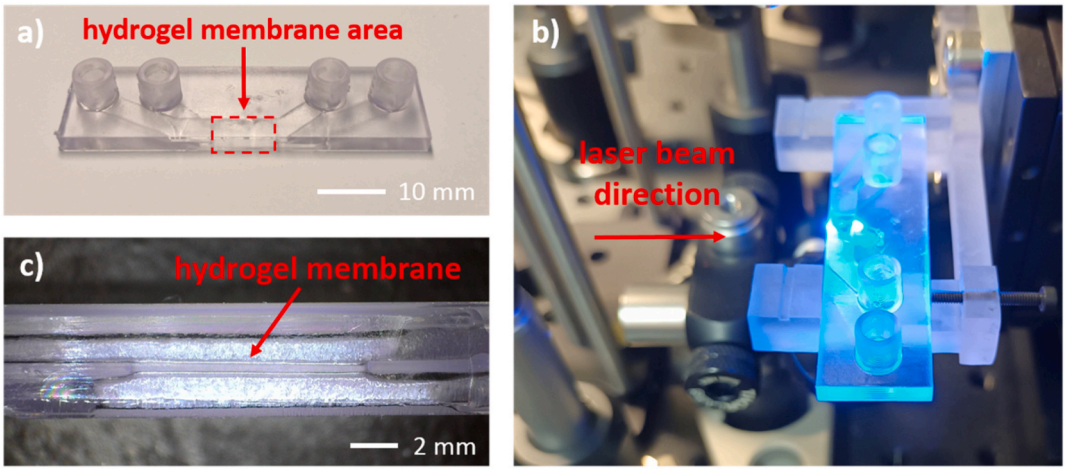

Fig. 6. a) 3D printed microfluidic chip with 2 channels, b) microfluidic chip under laser illumination to photopolymerize an hydrogel membrane, c) side-view of the microfluidic chip with the hydrogel membrane separating the 2 channels.

3.2. Lab-in-lab device

There is a growing interest in microfluidic devices for the biological domain to model micro-physiological interactions in so-called organ-on-chips (OOC) [18]. To be closer to a physiological behavior, the conventional microfluidic chips have to be functionalized by adding structured biomaterials such as hydrogels [19]. These biomaterials are much more representative of the properties of the extracellular matrix than standard OOC materials like polydimethylsiloxane (PDMS), thermoplastics or 3D printing resins. For example, hydrogels can be used as a membrane for 2D cell culture or to build more complex systems for 3D cell culture [20,21]. With our experimental setup (Fig. 6b), we polymerized an hydrogel membrane into a double-flow microfluidic chip (Fig. 6a) made with the Form 3B + printer and the BioMed Clear resin (FormLabs, MA, USA). This membrane can mimic the epithelial-endothelial barrier between the two microfluidic channels of the chip. The hydrogel was a 10% concentration gelatin methacrylate (Advanced BioMatrix PhotoGel®, CA, USA) with a 2% (w/w) LAP photoinitiator, sensitive to our blue laser (405 nm). The laser beam exposure time was 7s at 1.4 mW power level. The adjustable dimensions of the membrane are 1 cm long for a 350 μm thickness in the example shown in Fig. 6c). Due to the swelling properties of the hydrogel, this thickness can evolve depending on its environment (air, cell culture media). The hydrogel was injected in the chip through its channels. The unpolymerized parts was cleaned with dry air flow through these channels.

4. Concluding remarks and future scope

Combining holographic photopolymerization and microfluidics offers brand new opportunities of micro-fabrication. Real time 3D-printing can produce in one shot 3D architectured microchannels or free-standing complex micro-objects eventually in flow. The methodology can be seen as a lab-in-lab fabrication platform. It can be applied to *e.g.*, various types of photopolymerizable organics such as acrylates or biocompatible hydrogels.

As perspectives, future works will be focused on the exploration of the versatility of the technology. Interesting preliminary results were already obtained using other photopolymerizable feedstocks such as polymer-derived ceramics that can be further pyrolyzed to produce all-ceramic 3D micro-objects and lab-in-lab devices. We also started investigating the possibility to add functional and/or structural fillers to the feedstocks, such as nanoparticles.

Author contribution statement

Abhijeet Lale, Colman Buckley: Performed the experiments; Analyzed and interpreted the data; Wrote the paper.

Vincent Kermène, Fabrice Rossignol: Conceived and designed the experiments; Analyzed and interpreted the data; Wrote the paper.

Agnès Desfarges-Berthelemot, Frédéric Dumas-Bouchiat, Emmanuel Mignard: Analyzed and interpreted the data; Contributed reagents, materials, analysis tools or data.

Data availability statement

Data will be made available on request.

Declaration of competing interest

The authors declare the following financial interests/personal relationships which may be considered as potential competing interests:Fabrice ROSSIGNOL reports financial support was provided by French Regional Council of Nouvelle Aquitaine.

Acknowledgements

This research was performed with the financial support of the French Nouvelle Aquitaine Region (Holofluid-3D and 3DEFI projects). We want to acknowledge Pierre Lidon, Géérald Glisson and Pierre Guillot of the LOF laboratory (CNRS UMR 5258, Solvay, 178 Avenue du Dr Albert Schweitzer, 33600 Pessac, France) for their support in microfluidic technologies. We also want to acknowledge Nicolas Véédrenne and Florent Di Meo (INSERM U1248 Pharmacology & Transplantation, ΩHealth Institute - Univ. Limoges, 2 rue du Prof. Descottes, 87000 Limoges, France) for their support for the design of the double-flow microfluidic chip.

References

[1] N. Bhattacharjee, A. Urrios, S. Kanga, A. Folch, The upcoming 3d-printing revolution in microfluidics, Lab Chip 16 (2016) 1720–1742, https://doi.org/10.1039/c6lc00163g.
[2] S. Waheed, J.M. Cabot, N.P. Macdonald, T. Lewis, R.M. Guijt, B. Paull, M.C. Breadmore, 3d printed microfluidic devices: enablers and barriers, Lab Chip 16 (2016) 1993–2013, https://doi.org/10.1039/C6LC00284F.
[3] L. Yao, S. Weiwei, J. Lei, J. Quin, L. Bingcheng, Rapid prototyping of paper-based microfluidics with wax for low-cost, portable bioassay, Electrophoresis 30 (2009) 1497–1500, https://doi.org/10.1002/elps.200800563.
[4] D.T. Nguyen, C. Meyers, T.D. Yee, N.A. Dudukovic, J.F. Destino, C. Zhu, E.B. Duoss, T.F. Baumann, T. Suratwala, J.E. Smay, R. Dylla-Spears, 3d-printed transparent glass, Adv. Mater. 29 (2017), 1701181, https://doi.org/10.1002/adma.201701181.
[5] T.D. Ngo, A. Kashani, G. Imbalzano, K.T.Q. Nguyen, D. Hui, Additive manufacturing (3d printing): a review of materials, methods, applications and challenges, Compos. B Eng. 143 (2018) 172–196, https://doi.org/10.1016/j.compositesb.2018.02.012.
[6] A. Bhargav, V. Sanjairaj, V. Rosa, L.W. Feng, J.F. Yh, Applications of additive manufacturing in dentistry: a review, Journal of biomedical materials research. Part B, Applied biomaterials 106 (2018) 2058–2064, https://doi.org/10.1002/jbm.b.33961.
[7] H. Gong, B.P. Bickham, A.T. Woolley, G.P. Nordin, Custom 3d printer and resin for 18 μm x 20 μm microfluidic flow channels, Lab Chip 17 (2017) 2899–2909, https://doi.org/10.1039/c7lc00644f.
[8] J.P. Kirk, A.L. Jones, Phase-only complex-valued spatial filter, J. Opt. Soc. Am. 61 (1971) 1023–1028, https://doi.org/10.1364/JOSA.61.001023.
[9] S.A. Jahan, T. Wu, Y. Zhang, J. Zhang, A. Tovar, H. Elmounayri, Thermomechanical design optimization of conformal cooling channels using design of experiments approach, Procedia Manuf. 10 (2017) 898–911, 10.1016/j.promfg.2017.07. 078.
[10] C.W. Hull, Apparatus for Production of Three-Dimensional Objects by Stereolithography, US Patent, 1986, p. 4575330A.
[11] J.W. Choi, R. Wicker, S.H. Lee, K.H. Choi, C.S. Ha, I. Chung, Fabrication of 3D biocompatible/biodegradable micro-scaffolds using dynamic mask projection microstereo-lithography, J. Mater. Process. Technol. 209 (2009) 15–16, 10.1016/j.jmatprotec.2009.05.004.
[12] J.R. Tumbleston, D. Shirvanyants, N. Ermoshkin, R. Januszewicz, A.R. Johnson, D. Kelly, K. Chen, R. Pinschmidt, J.P. Rolland, A. Ermoshkin, E.T. Samulski, J. M. DeSimone, Additive manufacturing. continuous liquid interface production of 3d objects, Science 347 (2015) 1349–1352, https://doi.org/10.1126/science.aaa2397.
[13] M. Regehly, Y. Garmshausen, M. Reuter, N.F. König, E. Israel, D.P. Kelly, C. Chou, K. Koch, B. Asfari, S. Hecht, Xolography for linear volumetric 3d printing, Nature 588 (2020) 620–624, https://doi.org/10.1038/s41586-020-3029-7.
[14] D. Loterie, P. Delrot, C. Moser, High-resolution tomographic volumetric additive manufacturing, Nat. Commun. 852 (2020) 1–6, https://doi.org/10.1038/s41467-020-14630-4.
[15] M. Shusteff, A.E.M. Browar, B.E. Kelly, J. Henriksson, T.H. Weisgraber, R.M. Panas, N.X. Fang, C.M. Spadaccini, One-step volumetric additive manufacturing of complex polymer structures, Sci. Adv. 3 (2017) 1–7, https://doi.org/10.1126/sciadv.aao5496.
[16] B.E. Kelly, I. Bhattacharya, H. Heidari, M. Shusteff, C.M. Spadaccini, H. Taylor, Volumetric additive manufacturing via tomographic reconstruction, Science 363 (2019) 1075–1079, https://doi.org/10.1126/science.aau7114.
[17] N. Lorber, B. Pavageau, E. Mignard, Droplet-based millifluidics as a new miniaturized tool to investigate polymerization reactions, Macromolecules 43 (2010) 5524–5529, https://doi.org/10.1021/ma100233r.
[18] C.M. Leung, P. De Haan, K. Ronaldson-Bouchard, G.-A. Kim, J. Ko, H.S. Rho, Z. Chen, P. Habibovic, N.L. Jeon, S. Takayama, M.L. Shuler, G. Vunjak-Novakovic, O. Frey, E. Verpoorte, Y.-C. Toh, A guide to the organ-on-a-chip, Nat Rev Methods Primers 2 (2022), https://doi.org/10.1038/s43586-022-00118-6.
[19] H. Liu, Y. Wang, K. Cui, Y. Guo, X. Zhang, J. Qin, Advances in hydrogels in organoids and organs-on-a-chip, Adv. Mater. 31 (2019), 1902042, 10.1002/adma.201902042.
[20] S.R. Caliari, J.A. Burdick, A practical guide to hydrogels for cell culture, Nat. Methods 13 (2016) 405–414, https://doi.org/10.1038/nmeth.3839.
[21] D. Vera, M. García-Díaz, N. Torras, M. Álvarez, R. Villa, E. Martinez, Engineering tissue barrier models on hydrogel microfluidic platforms, ACS Appl. Mater. Interfaces 13 (2021) 13920–13933, 10.1021/acsami.0c21573.